Golgi localization of SARS-CoV-2 spike protein and interaction with furin in cerebral COVID-19 microangiopathy: a clue to the central nervous system involvement?

Susana Boluda, Karima Mokhtari, Bruno Mégarbane, Djillali Annane, Bertrand Mathon, Albert Cao, Clovis Adam, Alexandre Androuin, Franck Bielle, Guy Brochier, et al.

Original Paper

Golgi localization of SARS-CoV-2 spike protein and interaction with furin in cerebral COVID-19 microangiopathy: a clue to the central nervous system involvement?

Susana Boluda[1,2], Karima Mokhtari[1,2], Bruno Mégarbane[3], Djillali Annane[4], Bertrand Mathon[5], Albert Cao[6], Clovis Adam[7], Alexandre Androuin[2], Franck Bielle[1,2], Guy Brochier[1,8], Frédéric Charlotte[9], Lydia Chougar[10], Khalid Hamid El Hachimi[2,11], Marc Eloit[12], Stéphane Haïk[1,2], Dominique Hervé[13], Amal Kasri[2], Valentin Leducq[14], Stéphane Lehéricy[10], Etienne Levavasseur[1,2], Christian Lobsiger[2], Geoffroy Lorin de La Grandmaison[15], Isabelle Malet[14], Isabelle Malissin[3], Stéphane Marot[14], Serge Marty[2], Philippe Pérot[12], Isabelle Plu[1,2], Annick Prigent[2], Lev Stimmer[2], Marie-Claude Potier[2], Anne-Geneviève Marcelin[14], Benoît Delatour[2], Charles Duyckaerts[1,2], Danielle Seilhean[1,2]

[1] *Department of Neuropathology, Pitié-Salpêtrière Hospital, AP-HP Sorbonne University, Paris, France*

[2] *Institut du Cerveau - Paris Brain Institute - ICM, Inserm U1127, CNRS UMR7225, APHP, Sorbonne University, Pitié-Salpêtrière Hospital, Paris, France*

[3] *Department of Medical and Toxicological Critical Care, Lariboisière Hospital, AP-HP, Paris University, INSERM UMRS-1144, Paris, France*

[4] *Department of Critical Care, Raymond Poincaré Hospital, Boulevard Raymond Poincaré, APHP, Paris-Saclay University, INSERM U1173, Garches, France*

[5] *Department of Neurosurgery, Pitié-Salpêtrière Hospital, AP-HP Sorbonne University, Paris, France*

[6] *Department of Neurology, Neuro-ICU, Pitié-Salpêtrière Hospital, AP-HP Sorbonne University, Paris, France*

[7] *Department of Pathology, Bicêtre Hospital, AP-HP, Paris Saclay University, Le Kremlin-Bicêtre, France*

[8] *Institut de Myologie, Pitié-Salpêtrière Hospital, Paris, France*

[9] *Department of Pathology, Pitié-Salpêtrière Hospital, AP-HP Sorbonne University, Paris, France*

[10] *Department of Neuroimaging, Pitié-Salpètrière Hospital, AP-HP Sorbonne University, Paris, France*

[11] *Ecole Pratique des Hautes Etudes (EPHE), Paris Sciences et Lettres (PSL) University, Paris, France*

[12] *Institut Pasteur, Pathogen Discovery Laboratory, Paris, France*

[13] *Department of Neurology, Lariboisière Hospital, AP-HP Nord- Paris University, Paris, France*

[14] *Department of Virology, Pitié-Salpêtrière Hospital, AP-HP Sorbonne University, INSERM 1136, Institut Pierre Louis d'Epidémiologie et de Santé Publique (iPLESP), Paris, France*

[15] *Department of Forensic Medicine and Pathology, Raymond Poincaré Hospital, AP-HP, Paris Saclay University, Garches, France*

Corresponding author:
Danielle Seilhean · Department of Neuropathology · Pitié-Salpêtrière Hospital · AP-HP Sorbonne University · Paris · France
danielle.seilhean@gmail.com

Additional resources and electronic supplementary material: supplementary material

Submitted: 04 January 2023 · Accepted: 06 February 2023 · Copyedited by: Georg Haase · Published: 10. February 2023

Abstract

In a neuropathological series of 20 COVID-19 cases, we analyzed six cases (three biopsies and three autopsies) with multiple foci predominantly affecting the white matter as shown by MRI. The cases presented with micro-hemorrhages evocative of small artery diseases. This COVID-19 associated cerebral microangiopathy (CCM) was characterized by perivascular changes: arterioles were surrounded by vacuolized tissue, clustered macrophages, large axonal swellings and a crown arrangement of aquaporin-4 immunoreactivity. There was evidence of blood-brain-barrier leakage. Fibrinoid necrosis, vascular occlusion, perivascular cuffing and demyelination were absent. While no viral particle or viral RNA was found in the brain, the SARS-CoV-2 spike protein was detected in the Golgi apparatus of brain endothelial cells where it closely associated with furin, a host protease known to play a key role in virus replication. Endothelial cells in culture were not permissive to SARS-CoV-2 replication. The distribution of the spike protein in brain endothelial cells differed from that observed in pneumocytes. In the latter, the diffuse cytoplasmic labeling suggested a complete replication cycle with viral release, notably through the lysosomal pathway. In contrast, in cerebral endothelial cells the excretion cycle was blocked in the Golgi apparatus. Interruption of the excretion cycle could explain the difficulty of SARS-CoV-2 to infect endothelial cells *in vitro* and to produce viral RNA in the brain. Specific metabolism of the virus in brain endothelial cells could weaken the cell walls and eventually lead to the characteristic lesions of COVID-19 associated cerebral microangiopathy. Furin as a modulator of vascular permeability could provide some clues for the control of late effects of microangiopathy.

Keywords: COVID-19, Neuro-Covid, Microangiopathy, Furin, Blood-brain barrier (BBB)

Introduction

Many questions remain open regarding the frequent and diverse involvement of the central nervous system (CNS) by SARS-CoV-2 [11, 27, 49]. Inflammatory infiltrates have been found, especially in the brainstem [28], and have been taken as evidence of encephalitis [28, 54]. Nevertheless, in most cases, inflammation is inconspicuous or even absent [10, 15, 47]. In some cases, direct neuroinvasion by the virus has been suggested or observed. The virus may invade the brain through the olfactory mucosa and the nerve processes that cross the cribriform plate [13, 32]. Bitemporal necrosis found at CT scan and MRI, similar to the one seen in herpetic encephalitis, has been reported [34, 36, 43]. The presence of the virus genome has been demonstrated in the olfactory mucosa in a subset of patients (21 among 40 patients for Matschke et al.[28], four among 20 for Serrano et al.[47]). Although rarely, the SARS-Cov-2 virus genome has also been observed in various regions of the CNS including the olfactory bulb, brainstem, temporal cortex, amygdala and leptomeninges [28, 44, 47]. Even though the possibility of direct neuroinvasion has been confirmed by some experimental data [50], the viral genome turned out to be difficult to detect in the human CNS [47, 49], except in a recent study that found viral genome throughout the brain and other organs by droplet digital polymerase chain reaction (ddPCR)[52]. Multiple lesions evocative of acute disseminated encephalomyelitis (ADEM) have been described [37, 45]. Anti-aquaporin-4 circulating antibodies have been found as in *neuromyelitis optica* [8]. This observation emphasizes the role of secondary immune mechanisms and downplays the direct impact of the virus in the CNS.

Large vessel occlusions occur especially in young COVID-19 patients [26, 40]. In some cases, the lesions also involve the brain microvasculature. These cases of COVID-19 associated cerebral microangiopathy (CCM) present with multiple, often hemorrhagic lesions, evocative of small artery disease [6, 7, 22]. Histopathological studies show micro-infarcts, the mechanism of which is still under debate [16, 18, 21, 24]. In the present paper, six cases of CCM were histopathologically examined and the mechanisms of the lesions were investigated. While these cases did not display viral genomes or viral particles detectable by molecular techniques, they

showed the presence of spike protein (SP) in the endothelial vessels. SP protein was consistently associated to furin. Furin is a serine protease involved in the metabolism of the spike protein (SP) of SARS-CoV-2. It cleaves SP and plays a key role in virus entry and viral protein biogenesis [17, 20, 39, 48]. We investigated the subcellular localization of furin and SP in the lesions of CCM

Material and Methods

Patients

The study received approval from the Sorbonne University Ethic Committee (CER-202028). Twenty cases of acute COVID-19 infection collected during 2020, corresponding to the first two waves of the pandemic, were analyzed: 13 cases in the neuropathology department of Pitié-Salpêtrière Hospital (ten autopsies and three cerebral biopsies); seven others in the pathology department of Bicêtre Hospital, after autopsy at Raymond Poincaré Hospital, Garches. A Magnetic Resonance Imaging (MRI) was performed either *ante-mortem* or *post-mortem* in all the Pitié-Salpêtrière cases and *ante-mortem* in one patient from Bicêtre Hospital. For those cases in Bicêtre Hospital without MRI, inclusion was based on histopathological criteria. The three biopsied cases (patients # 1 to 3, Table 1, Fig.1) and two autopsied cases (patients # 4 and 5), presented with multifocal hypersignals in the deep white matter, evocative of microbleeds. Microbleeds were seen in patient # 6 at histopathological examination (Table 1, Fig. 1, Supplementary table).

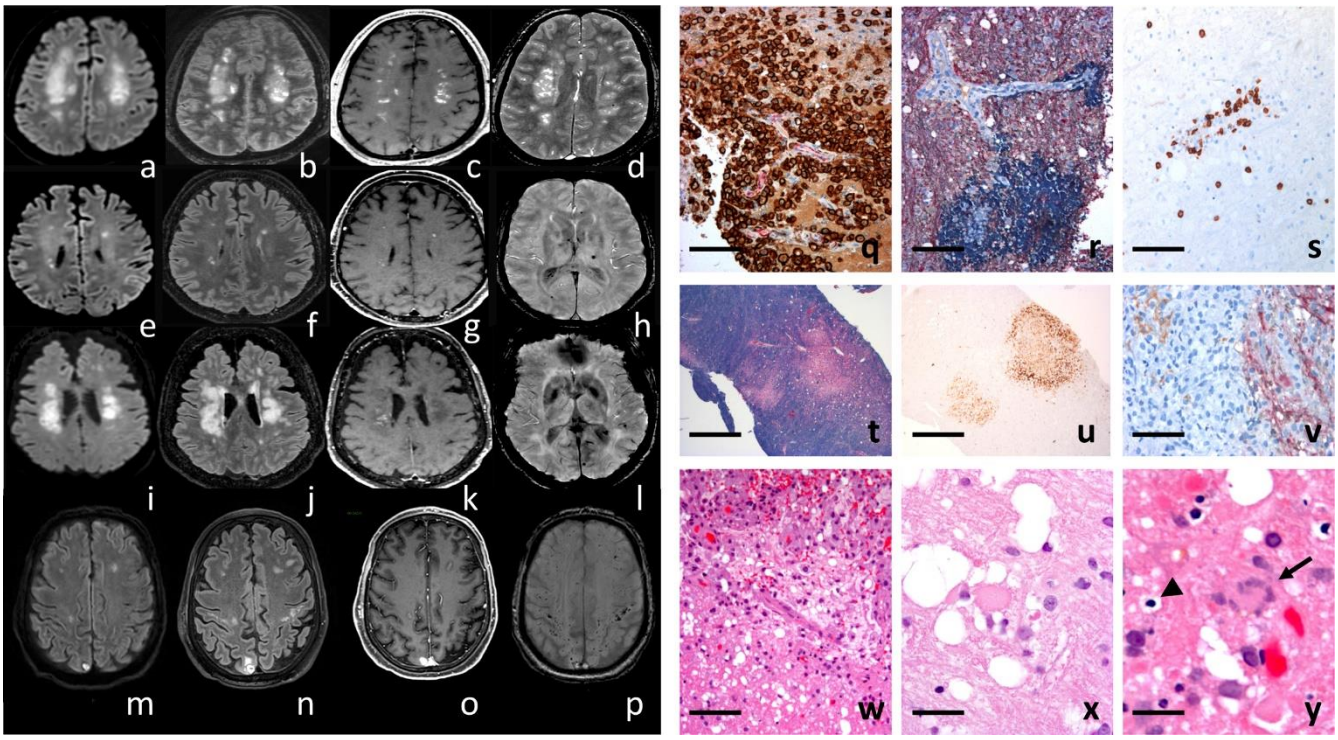

Fig 1. Cerebral microangiopathy with multiple microhemorrhagic foci. Magnetic resonance imaging. Case # 1 (a - d), Case # 2 (e - h), Case # 3 (i - l) and Case # 4 (m - p). Multi-territory recent ischemic lesions with reduced apparent diffusion coefficient were detected on DWI diffusion-weighted (left column a, e, i, m) and FLAIR images (middle left column, b, f, j, n), with frequent contrast enhancement on T1-weighted images (middle right column, c, g, k, o). Susceptibility-weighted images showed numerous microbleeds in cortico-subcortical areas and deep hemispheric white matter (SWI, right column, d, h, l, p). **Brain biopsies.** Case # 1 (q-s), case # 2 (t-v), case # 3 (w-y). (q) SMA (red)-CD163 (brown) double labeling showing a macrophagic infiltrate around a vessel; (r) MBP (brown)-NF (red) with hematoxylin (blue) counterstain showing no demyelination but bleeding; (s) A few CD8+ lymphocytes are observed within the microhemorrhagic foci (q, r, s : *scale bars* = 80 µm). Needle biopsy sample showing focal lesions in the white matter: (t) HE-Luxol fast Blue; (u) CD163 for macrophages (t, u: *scale bar* = 400 µm). (v) MBP (brown)-NF (red) with hematoxylin (blue) counterstain showing an area rich in macrophages without accumulation of myelin debris (*scale bar* = 40 µm). (w) Foci of vacuolated tissue around a vessel (H&E, *scale bar* = 80 µm). (x) Axonal damage was severe within the foci with numerous axonal swelling and vacuolization; (y) at the periphery of the lesion occasional glial nuclear alterations (arrow), and apoptotic nuclei (arrow head) were noticed (x, y: H&E, *scale bars* = 20 µm).

Table 1: Clinical data

BMI, body-mass index; CSF, cerebrospinal fluid.

	Patient 1	Patient 2	Patient 3	Patient 4	Patient 5	Patient 6
Age	37	49	77	63	51	52
Gender	M	M	F	M	M	M
Ethnicity	Indian	North African	North African	White European	Sub-Saharan African	White European
Risk factors	Obesity (BMI =31)	Rheumatoid purpura; renal insufficiency; kidney transplantation	Hypertension, obesity, asthma	Hypertension	Hypertension	Obesity BMI=37 hypertension
Day 0: demand for medical care	Dry cough, odynophagia, headache	Fever, cough, dyspnea	Fever, fatigue, cough, dyspnea, headache, anosmia	Fever, dyspnea	Fever, cough and dyspnea	Fever, cough, dyspnea
Chest CT scan	Bilateral multifocal ground glass pattern					
Persistent consciousness alteration after sedative drug discontinuation	Day 33	Day 30	Day 22	Day 15	Day 7	N/A
CSF analysis	Pleiocytosis (10 cells/mm^3) normal protein and glucose levels	Normal				N/A
SARS-CoV RT-PCR on CSF	Negative					
Brain MRI	Multiple confluent FLAIR hyper signals in the white matter, most of them with contrast enhancement and central cavitation. Some micro bleeds were also observed in supra and infra tentorial regions. (Fig1. a)	Multiple small diffusion hyper intensities in the deep white matter and brainstem, associated with micro bleeds in supra and infra tentorial regions. A lacunar infarct was observed in the left thalamus. (Fig1. b)	Multiple confluent FLAIR hyper signals in the deep supratentorial white matter, mostly with necrotic centers and slight peripheral enhancement. (Fig1. c)	Multi-territory recent ischemic lesions, an acute cerebral hemorrhage and innumerable microbleeds in the cortico-subcortical and deep hemispheric white matter were detected respectively on FLAIR, DWI and SWI sequences. (Fig 1. d-i)	Early MRI showed strong bilateral abnormal T2-FLAIR HI without post gadolinium enhancement within the olfactory bulb and tract. T2-FLAIR*hyperintensity of the cerebrospinal fluid on the border of the medulla oblongata, pons, mesencephalon, suggesting a leptomeningitis. No post gadolinium enhancement of leptomeninges.	N/A
Electro-encephalogram (EEG)	Nonspecific diffuse slow-wave activity, unreactive, without any epileptic patterns	Fluctuating slow waves, predominantly affecting the anterior areas	Nonspecific diffuse slow-wave activity, inconstantly reactive, without any epileptic patterns	Slow, with disorganized background activity, little reactive without any epileptic patterns	Slow activity with centro-temporal slow delta waves	N/A
Cerebral biopsy	Day 38	Day 53	Day 34	No	No	No

	Patient 1	Patient 2	Patient 3	Patient 4	Patient 5	Patient 6
Treatment	Plasma exchanges and corticosteroids [3]	Corticosteroids, catecholamine infusion, hemodialysis and veno-venous ECMO on day 43			Cefotaxime, Spiramycine, Lopinavir/Ritonavir. Sedation with midazolam, sufentanyl, propofol, mechanical ventilation vasopressive therapy, hemodialysis, heparin	Cefotaxime, Azithromycine, hydroxychlorquine. Sedation with midazolam, sufentanyl, propofol, mechanical ventilation, vasopressive therapy, hemodialysis, ECMO
Course of the disease	No consciousness improvement	Communication was restored on day 63. On day 69, he could swallow; tracheostomy was withdrawn and ventilation was discontinued.	No consciousness improvement	Multiple organ failure	No consciousness improvement, multiple organ failure	Refractory hypoxia, multiple organ failure
Death	Day 81	No	Day 75	Day 44	Day 20	Day 11
Autopsy	No	-	No	Yes	Yes	Yes
Post mortem delay (hours)	-	-	-	35	15	100
Brain weight (grams)	-	-	-	1370	1475	1679

Table 1: Clinical data

Regarding the remaining autopsied cases, three presented with deep venous thrombosis and the others did not show CNS involvement on MRI. In total, six cases of COVID-19 infection with white matter anomalies were analyzed in the present study.

The clinical histories of the selected patients showed similarities and are summarized in Table 1. The age of the patients ranged from 37 to 77 years (mean: 54.8 years). All of them were males, except for patient # 3. They all presented at least one risk factor: obesity, hypertension or both, but none of them was diabetic. Patient # 2 was under immunosuppressive treatment as he had a kidney transplantation. Seven to ten days after the first COVID-19 symptoms, the patients were admitted to the hospital with acute respiratory distress syndrome. Diagnosis was made by detecting SARS-CoV-2 RNA with Real Time-Polymerase Chain Reaction (RT-PCR) in samples from nasopharyngeal swabs. The patients were sedated, mechanically ventilated and received corticosteroids and supportive care, which improved their respiratory conditions seven to 33 days later. Despite sedative drug discontinuation, awakening was unsatisfactory: the patients opened their eyes spontaneously but they did not respond to simple orders. Brainstem reflexes were preserved. Skew eye deviation and left internuclear ophtalmoplegia were observed in patient # 2. No alternative metabolic or drug-related causes were found to explain impaired consciousness. Patients # 2 and 6 were treated with extracorporeal membrane oxygenation (ECMO). Multiple punctate lesions predominating in the white matter were seen in patients # 1 to 5, for whom MRI was available (Fig. 1, a-p). The therapeutic management of patients # 1 to 3 has been described in a previous work [4].

Control samples

Autopsy samples from 16 cases with various conditions were used as controls. They included samples from normal brains (n=4), COVID-19 patients without brain lesions (n=4), cases with acute disseminated encephalomyelitis (ADEM, n=1) or multiple sclerosis (n=1) and cases with vascular lesions of various causes: watershed infarcts (n=2),

post ECMO hypoxemia (n=2), endovascular lymphoma (n=1), amyloid microangiopathy Thal type 1 (n=2), in which recent hemorrhages and ischemic lesions were seen. Immunohistochemistry for spike protein and furin was done in the frontal white matter, striatum and brainstem in all cases.

Biopsy and autopsy tissue processing

The autopsies were authorized according to French current regulation and the use of samples for research was authorized by the next of kin. The samples were collected and stored according to the COVID tissue bank (COVITIS) protocol, approved by the national biomedical agency and the French Ministry of Research (Agence de la Biomédecine, PFS 20-008; French Ministry of Research DC2020-4022). The protocol includes sampling of the brain, lungs, heart, trachea, lymph nodes, tonsils, spleen, liver, pancreas, guts, bladder, kidneys, skin, muscles, nerves and bone marrow. Each sample was prepared in three ways: 1) fixed in formaldehyde and paraffin embedded (FFPE); 2) snap frozen in liquid nitrogen cooled isopentane for cryostat sections; 3) directly frozen at -80 °C for molecular biology. In cases # 5 and 6 the frozen extra-cerebral samples were limited to the lung.

For brain sampling, the cerebral hemispheres were separated immediately after removal by a section across the *corpus callosum*; the sagittal section was extended to the brainstem and the cerebellum. The right hemi-brain was sliced into coronal sections. Samples from the olfactory bulb and piriform gyrus, frontal, temporal, occipital and hippocampal cortices, *corona radiata* white matter, striatum, thalamus, amygdala, cerebellum, mesencephalon, pons, medulla oblongata and leptomeninges were fast-frozen at -80°C. Nearby samples were fixed for 15 days in buffered 4% formaldehyde, then immersed one hour in formic acid (a systematic measure in the laboratory to decrease the infectivity of a potential prion disease), before paraffin embedding, cutting and staining. The left hemi-brain was immersed for one month in buffered 4% formaldehyde and the same regions as in the right hemi-brain were sampled. After one-hour immersion in a 90% formic acid solution, the samples were embedded in paraffin and cut at a thickness of 3 µm.

The biopsy samples were fixed for eight hours in 4% formaldehyde, directly embedded in paraffin without a formic acid pretreatment and cut at a thickness of 4 µm. In cases # 1 to 4, brain tissue was fast frozen at -80°C for Next Generation Sequencing (NGS).

Staining and immunohistochemistry (IHC)

Tissue sections from the biopsy samples and selected regions of the autopsy cases were stained with hematoxylin-eosin (H&E), Perls' method, orcein, Masson's trichrome, Martius Scarlet Blue, periodic acid Schiff (PAS), Gram's and Grocott's technique. In addition, sections from selected regions of the autopsy cases were stained with H&E combined with Luxol Fast Blue. Some sections were immunostained with a Ventana BenchMark stainer (Roche™). The biotinylated secondary antibody was included in the detection kit (Ventana Medical Systems Basic DAB Detection Kit 250-001). Diaminobenzidine (DAB), occasionally combined with alkaline phosphatase (ALP) for double labelling, was used as a chromogen. The pretreatment and the antibodies used for IHC are listed in table 2.

Multispectral microscopy

FFPE sections from the frontal cortex (case # 4) were doubly immunostained against SARS-CoV-2 SP (DAB chromogenic substrate) and giantin (Fast Red - FR - chromogen). To separate DAB and FR signals, the sections were analyzed with the Mantra™ multispectral imaging station and the Inform software (Akoya Biosciences). DAB and FR signals were each associated with a pseudo-color in order to distinguish SP and giantin immunolabelling.

Confocal microscopy

To determine the intracellular localization of SP protein in the cells and its interaction with furin, FFPE sections from the frontal cortex of cases # 4, 5 and 6 and from the lung (case # 4) were immunostained with the SP antibody (revealed with secondary antibody coupled with Alexa Fluor-AF488), and doubly labelled with antibodies against BIP, giantin, furin, TGN46 or cathepsin B (Table 2), revealed with secondary antibody coupled with Alexa Fluor-AF555. The sections were counterstained with DAPI. Distribution and colocalization of immunofluorescent signals were analyzed with a confocal microscope (Leica SP8 DLS).

Table 2: Immunohistochemical methods

CC1, a proprietary high pH (=8) buffer at 95°C; **CC2**, a proprietary pH (=6) buffer; **FA**: formic acid; **RT**: room temperature.

Antigen	Poly/mono-clonal	Producer	Immunogen	Clone	Pretreatment	Dilution	Incubation time
Aβ	Monoclonal (mouse)	Dako®	Deposits of beta-amyloid	6F/3D	Formic acid	1:200	Overnight RT
Angiotensin conversion enzyme-2 (ACE2)	Polyclonal (rabbit)	Abcam®	Synthetic peptide within Human ACE2 aa 750 to the C-terminus	–	CC1® 64 min	1:1500	60 min
Aquaporin-4 (AQP4)	Polyclonal (rabbit)	Sigma®	Aquaporin-4 water channel	–	CC2®	1:3000	32 min
BIP GRP78	Polyclonal (rabbit)	Abcam®	Synthetic peptide	–	CC1® 52 min	1:200	60 min
Cathepsin B	Polyclonal (rabbit)	Calbiochem®	Lysosomes	Ab-3	CC1® 52 min	1:200	60 min
CD147/basigin	Monoclonal (rabbit)	Abcam®	Synthetic peptide	EPR4053	CC1® 36 min	1:500	Overnight +4°C
CD163	Monoclonal (mouse)	Cell Marque®	Acute phase-regulated transmembrane protein on monocytes	MRQ-26	CC1® 64 min	1:50	32 min
CD20	Monoclonal (mouse)	Dako®	Transmembrane protein expressed on B cells	L26	CC1® 36 min	1:100	32 min
CD3	Monoclonal (rabbit)	Ventana®	Epsilon chain of the human CD3	2GV6	CC1® 30 min	prediluted	32 min
CD34	Monoclonal (mouse)	Dako®	Human endothelial cells	QBEend10	CC1® 30 min	1:50	20 min
CD4	Monoclonal (mouse)	Dako®	T helper cells	4B12	CC1® 36 min	1:40	60 min
CD8	Monoclonal (mouse)	Dako®	Suppressor/ cytotoxic T cells	C8/144B	CC1® 8 min	1:50	32 min
Cytomegalo-virus	Monoclonal (mouse)	Dako®	CMV immediate early antigen and early antigen	CCH2+ DDG9	Protease 4 min	1:50	32 min
Fibrinogen	Polyclonal (rabbit)	Dako®	Fibrinogen, fibrin and the fibrinogen fragments D and E	–	–	1:500	32 min
Furin	Monoclonal (rabbit)	Abcam®	Recombinant human furin	EPR14674	CC1® 52 min	1:100	60 min
GFAP	Monoclonal (mouse)	Dako®	Glial Fibrillary Acidic Pro-tein	6F2	–	1:500	28 min
Giantin	Polyclonal (rabbit)	Abcam®	Cis-media cisternae of the Golgi complex	–	CC1® 52 min	1:200	60 min
HSV1	Monoclonal (mouse)	Roche®	ICP8	10A3	CC1® 36 min	prediluted	32 min
IgG	Polyclonal (rabbit)	Dako®	–	–	–	1:40	120 min
Measles	Rabbit IgG	Quartett®	–	–	CC1® 56 min	1:40	60 min
Myelin basic protein (MBP)	Monoclonal (rabbit)	BioSB®	–	EP207	CC1® 36 min	1:50	60 min

Antigen	Poly/mono-clonal	Producer	Immunogen	Clone	Pretreatment	Dilution	Incubation time
Neurofilament (NF)	Monoclonal (mouse)	Dako®	70 kDa subunit of neurofilament (axons)	2F11	CC1®	1:2000	32 min
p62	Mouse IgG	BD Biosciences®	P62-lck ligand	3/p62	CC2® 44 min	1:500	1 h 36
Polyomavirus	Polyclonal (rabbit)	Courtesy Dr Walker, Madison, WI	Large T antigen	–	CC1®	1:500	32 min
SARS-CoV	Monoclonal (mouse)	Abcam®	Spike protein	3A2	CC1® 36 min	1:100	60 min
SARS-CoV2	Monoclonal (rabbit)	Clinisciences®	Nucleocapsid (N) protein	019	CC1® 36 min	1:100	32 min
Smooth muscle actin (SMA)	Monoclonal (mouse)	Dako®	N-terminal of the α smooth cell actin	1A4	CC1® 8 min	1:500	20 min
Tau	Monoclonal (mouse)	ThermoFisher®	Phospho-Tau (Ser202, Thr205)	AT8	CC1® 8 min	1:500	32 min
TGN46	Polyclonal (rabbit)	ThermoFisher®	Trans-Golgi network		CC1® 20 min	1:400	32 min
Toxoplasma gondii	Polyclonal (rabbit)	Biogenex®	–	–	CC1® 8 min	prediluted	32 min
Varicella-Zoster-virus	Monoclonal (mouse)	Monosan®	–	7 clones cock-tail	–	prediluted	32 min

Table 2: Immunohistochemical methods

Electron microscopy

In patient # 4, 1-mm^3 samples from altered white matter were fixed immediately with glutaraldehyde (2.5%, pH 7.4), post fixed with osmium tetroxide (2%), dehydrated and embedded in resin. Ultra-thin sections were obtained at different depths from three blocks and stained with uranyl acetate and lead citrate. The grids were observed using a Hitachi HT 7700 electron microscope (Elexience™, Verrières-le-Buisson, France) operating at 100kV.

Molecular SARS-CoV-2 analyses

Various morphological methods (*in situ* hybridization-ISH, RNAscope) and non-morphological methods (RT-PCR, NGS) were used to detect SARS-CoV-2 virus RNA in the tissues.

RT – PCR (Real time polymerase chain reaction)

To detect viral RNA in cases # 1 to 3, samples snap-frozen at -80°C were used. In case # 4, for which abundance of tissue was available, samples snap-frozen at -80°C from nine regions of the central nervous system and from multiple extra cerebral tissues were tested (Table 3). Total RNA was extracted with the RNeasy mini kit (Qiagen™), after a mechanical disruption with TissueLyserLT (Quiagen™). Total RNA samples were treated by DNase to avoid residual genomic DNA contamination. RT-PCR was subsequently performed using the RealStar SARS-CoV-2 RT-PCR kit (Altona diagnostics™) to estimate the SARS-CoV-2 viral load.

Next Generation sequencing (NGS)

NGS-based transcriptomic analysis to search for viral transcripts was used in tissue samples from four cases (cases # 1 to 4) as previously described [42]. This technique is agnostic and provides sequences of the human transcriptome, possibly mixed with exogenous sequences of pathogens. Those are identified by comparison with the sequences of known microbes. In addition, NGS-based target capture was used to increase the sensitivity towards SARS-CoV-2 RNA (Twist Biosciences™, San Francisco, USA).

ISH (in situ hybridization)

To explore further the presence of virus in various tissues, ISH was performed as previously described [42] on FFPE sections of lung and frontal lobe

in case # 4. ViewRNA ISH Tissue Assay Kit 2-plex (Thermo Fisher Scientific™) was used with a cocktail of custom branched DNA (bDNA) probes targeting six segments of known opening reading frames (ORFs) for COVID-19 Wuhan-Hu-1 strain based on GenBank MN909847 and a mix of control probes targeting human GAPDH, ACTB and PPI transcripts. The oligonucleotide probes were conjugated to alkaline phosphatase. Chromogens were Fast Red (for SARS-CoV-2 probe) and Fast Blue (for the control probes).

Table 3: Post mortem RT PCR autopsy case # 4

Organ/region		RT PCR result
Cardio-respiratory system	Right lung	+
	Left lung	+
	Trachea	–
	Myocardium	–
Hematopoietic organs	Mediastinal lymph node	+
	Cervical lymph node	+
	Spleen	+/–
	Bone marrow	–
	Tonsil	–
Digestive system	Tongue	–
	Esophagus	–
	Small intestine	–
	Colon	–
	Liver	–
	Pancreas	–
Urinary tract	Kidney	–
	Bladder	–
Muscle and nerve	Brachial plexus	–
	Deltoid	–
Central nervous system	Leptomeninges	–
	Frontal lobe (F2)	–
	Temporal lobe (T1)	–
	Hippocampus	–
	Calcarin	–
	Caudate nucleus	–
	Thalamus	–
	Cerebellum	–
	Olfactory bulb	–

RNAscope

In another attempt to detect viral RNA in the autopsy samples fixed for 15 days, FFPE RNA ISH was performed using the RNAscope ™ SARS-CoV-2 probes for the S gene encoding SP (catalogue #848561, Advanced Cell Diagnostics™) and the RNAscope ™ 2.5 HD Reagent Kit-BROWN™ (catalogue #322300). RNA integrity in tissue samples was controlled by a preliminary step using the RNAscope ™ Positive Control Probe - Hs-UBC (catalogue #310041). All experiments were carried out manually according to the manufacturer's instructions.

Cell Culture

To improve our understanding of the interaction of the virus with endothelial cells and furin, cultures of four cell lines were used: human endothelial cells derived from Induced pluripotent stem cells (iPSC-d-ECs), a human cerebral microvessel endothelial cell line (hCMEC/D3), a Human Umbilical Vein Endothelial Cell line (HUVEC) and a primate kidney cell line (Vero E6 cells).

The control iPSC-d-ECs line (Welcome Trust Sanger Institute, HipSci, Cell line name: bHipSci0914i-zerv_8 catalogue number: 77650327) was differentiated into endothelial cells from an *in vitro* monolayer following a previously developed protocol [41]. After differentiation, the iPSC-d-ECs were purified using Fluorescence Activated Cell Sorting (FACS). Cells were incubated with either Alexa Fluor 488-conjugated CD31 (PECAM1) antibody for 30 minutes, or isotype-matched secondary antibody in the absence of primary antibody serving as negative control. The purified iPSC-d-ECs were expanded in Endothelial Growth Medium-2 (EGM-2 Bullet kit, #cc86 3202, Lonza ™) and characterized by immunofluorescence for the expression of the endothelial markers CD31/PECAM1, CD144/VE-cadherin and von Willebrand factor. The hCMEC/D3 was kindly donated by P. O. Couraud from the Cochin Institute, Université de Paris, France. It was derived from microvessels obtained from tissue excised during surgery for epilepsy. The cells were immortalized by lentiviral transduction with the catalytic subunit of human telomerase (hTERT) and SV40 large T antigen [56]. These cells, which express a brain endothelium phenotype, were cultured as previously described [55].

iPSC-d-ECs and hCMEC/D3 were grown on surfaces coated with Matrigel (Corning™ #354277) or Type I Collagen (Corning™, #354236: Collagen I, Rat Tail Natural 100mg), respectively. The cells were cultured at 37°C with 5% CO2 in EGM-2 medium, supplemented with 0.1% penicillin-streptomycin (P/S; Gibco™).

HUVEC cells (a gift from the lab of Pr. Yong Chen) were grown at 37°C with 5% CO2 in EGM™ -2 BulletKit™ Medium with 0.1% P/S. At passage 7 the cells were seeded on 12-well plate on coverslips (12 mm).

Vero E6 cells (ATCC No. CRL-1586) correspond to a cell line isolated from kidney epithelial cells of African green monkey. The cells have lost the type I interferon gene cluster and are particularly sensitive to viral infection. They were used as controls for the *in vitro* infection by SARS-CoV-2 viruses. The line was cultured in Dulbecco's modified Eagle's medium (DMEM), supplemented with 10% fetal bovine serum (FBS), 1% non-essential amino-acids and 1% P/S (Gibco™).

In vitro infection of iPSC-d-EC and hCMEC/D3 cell line

iPSC-d-ECs at passage 2 (p2) or hCMEC/D3 cell line at p33 were seeded on coated glass coverslips. At 50 % of confluence, the iPSC-d-EC or hCMEC/D3 were incubated with 0.1, 0.5 and 1 multiplicities of infection (MOI). The supernatants and the cells were harvested at 48, 72 and 96 hours. Viral RNA (gene E) was quantified by RT-PCR in the supernatant and in the intra-cellular compartment. Vero E6 cells were used as controls.

Cell fixation and Immunofluorescence

The cells were fixed with phosphate buffer saline (PBS)-4% paraformaldehyde (Electron Microscopy Sciences) at room temperature, then quenched for 10 minutes with 50 mM PBS-NH_4CL. For permeabilization, cells were incubated in PBS supplemented with 2 g/L bovine serum albumin (BSA) and 0.5 g/L saponin for 20 minutes at room temperature. The antibodies were diluted in the permeabilization buffer. The cells were immunostained with the polyclonal rabbit anti-SP antibody (Abcam, #ab272504, 1:300) for one hour in a humid chamber at room temperature. After washes with PBS, the cells were incubated with Alexa Fluor-555 anti-rabbit secondary antibody (1:500) and co-stained with DAPI (Vector Laboratories, 1:10000). Slides were mounted in Vectashield™ antifade medium and observed with a Nikon A1R HD25 confocal microscope with resonant scanning at the x60 objective.

Cell incubation with SP peptides

HUVEC cells were incubated with recombinant SP S1 full length peptide (Val16-Arg685 ; ProSci #10-300) and control RBD peptide (Arg319-Phe541 ; ProSCi #10-303), as described in Nuovo et al. [38]. In brief, cells were incubated with 70ng/ml of S1 and RBD peptide for 48 hours. Cell fixation was performed with paraformaldehyde 4% for 10 min at room temperature. For permeabilization, cells were incubated in PBS supplemented with BSA 2g/L and saponin 0.5g/L for 20 min at room temperature. Rabbit anti -S1 (ProSCI 9083) and anti RBD (ProSCI 9087) were incubated in the permeabilization buffer. The secondary antibody was an anti-rabbit conjugated to Alexa Fluor 568. Coverslips were mounted in VECTASHIELD antifade mounting medium.

Results

Microangiopathy seen as microhemorrhages of small arteries is a common trait in a subset of SARS-CoV-2 infected patients.

As mentioned previously, radiological findings shared common features in the cases for whom MRI was available (Fig. 1, a-p). The same was true for neuropathology.

In the biopsy samples, multiple well-delineated foci of CD163 positive macrophages were observed in the white matter (Fig. 1. q, t, u, v). Macrophages were clustered around small caliber blood vessels (Fig. 1. q, r, w). They were not laden with luxophilic, Myelin Basic Protein (MBP) positive debris, nor was there myelino-axonal dissociation (Fig. 1. r, v). CD3 CD8 positive T lymphocytes were scattered among the macrophages and around the foci (Fig 1. s). In the foci, numerous and large axonal swellings were seen and white matter was vacuolized (Fig. 1. x). At the periphery of the lesions, apoptotic nuclei and

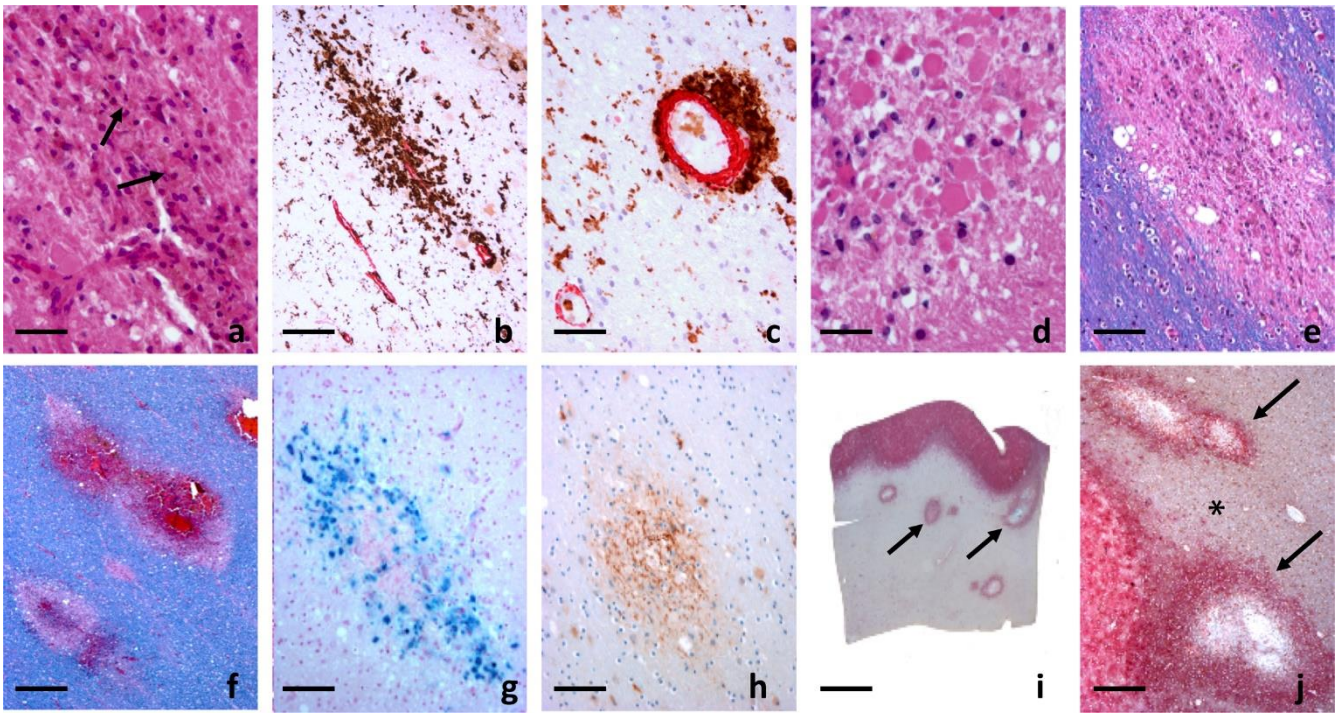

Fig 2. Case # 4 : neuropathology. (a) Small foci of necrosis in the white matter were centered by a small caliber blood vessel. H&E (a : *scale bar* = 40 µm). (b and c) Double labelling of SMA (in red) and of CD163 (in brown) labeled the compact wall of an arteriole surrounded by macrophages (b: *scale bar* = 80 µm; c: *scale bar* = 40 µm). (d and e) Within the foci, swollen axons were numerous (d: HE; *scale bar* = 20 µm), associated with a vacuolization of the cerebral tissue (e: HE-Luxol; *scale bar* = 80 µm). (f) Some lesions were centered by a recent hemorrhage (f: HE-Luxol; *scale bar* = 80 µm). (g) Perls positive siderophages indicated older bleedings (g: *scale bar* = 80 µm). (h) Fibrinogen immunoreactivity was evidence of blood brain barrier leakage (h: *scale bar* = 80 µm). (i) AQP4 immunoreactivity showed positive rings (arrows) in the subcortical and deep white matter (i: *scale bar* = 5 mm). (j) Large reactive astrocytes formed AQP4 positive rings around the lesions (arrows), contrasting with the depletion of AQP4 in the surrounding white matter - * (j: *scale bar* = 400 µm).

occasional glial nuclear alterations, reminiscent of Creutzfeldt-Peters cells, were seen (Fig. 1. y). Some recent blood extravasation (Fig. 1. r) and a few siderophages were observed. There was no fibrinoid necrosis or inflammatory cells seen within the vessel walls. We did not observe vascular occlusion, lymphocytic perivascular cuffing or neuronophagia. IHC against the proteins of herpes simplex virus 1, cytomegalovirus, varicella-zoster virus, polyomavirus, measles and *toxoplasma gondii* was negative, as was negative ISH with the Epstein-Barr virus EBER probe.

The lesions observed on the biopsies were more thoroughly studied in the autopsy cases that provided more material. Macroscopic examination of the three autopsied brains was characterized by multiple hemorrhages scattered in the deep and subcortical white matter. In case # 4 these were predominant in the supramarginal gyrus, first and second temporal gyri, where they were particularly numerous, and also in the pons and cerebellum. There was a 4 mm hemorrhage in the left occipital pole. In cases # 5 and # 6 the hemorrhages were predominant in the frontal lobe with additional bleeds in the striatum (case # 5) and in the pons (case # 6).

Microscopic examination of the autopsied cases showed similar lesions as those seen in the biopsies. The most conspicuous lesions were small foci rich in CD163 positive macrophages centered by a small caliber arteriole (Fig. 2. a, b, c) associated with swollen axons and vacuolization of the surrounding white matter (Fig. 2. d, e). As in the biopsies, there was no lymphocytic perivascular cuffing, demyelination, vascular occlusion or fibrinoid necrosis. Compared to biopsy cases, perivascular bleeding was more frequent and of different age (Fig. 2. f, g). Fibrinogen and IgG IHC were positive in the lesions, evidencing blood-brain barrier leakage (Fig. 2. h). Large reactive astrocytes formed aquaporin-4 (AQP4) positive rings around the lesions, contrasting with a low immunoreactivity in the normal looking white matter (Fig. 2. i, j). Aβ IHC was negative indicating absence of amyloid angiopathy. In summary,

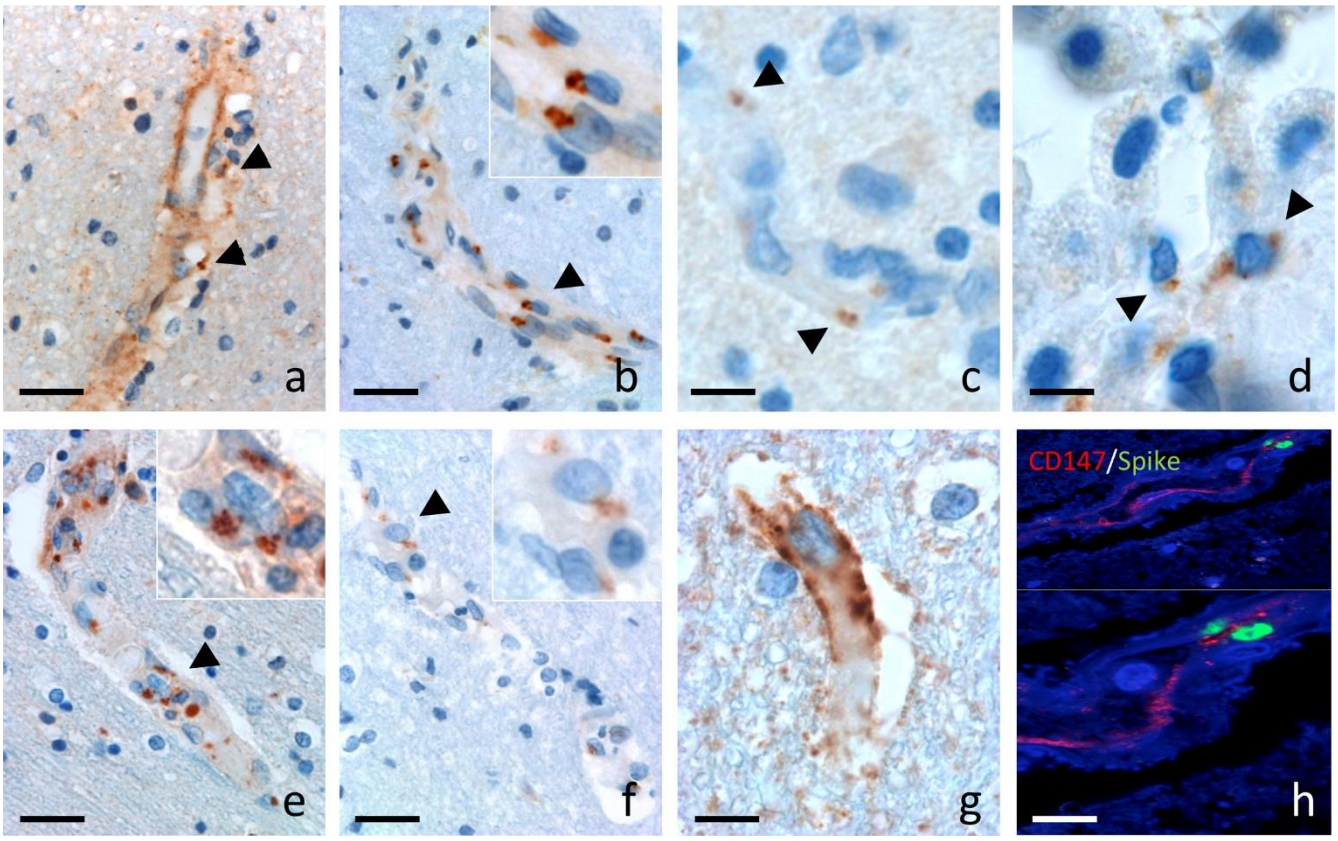

Fig 3. Localization of SARS-CoV-2 in brain tissue (case # 4). (a and b) SARS-CoV-2 was detected in the endothelial cells with two different antibodies (a, b: *scale bars* = 20 µm). With the anti-N antibody from Cliniscience™ the immunoreactivity was predominant in endothelial cells, with a diffuse endothelial labelling and paranuclear enhancement (a, arrowhead). With the Abcam™ anti-SP antibody, immunoreactivity was limited to the endothelial cells with paranuclear inclusions (b, arrowheads). Inset: higher magnification of cells indicated by arrow heads. (c) Immunoreactivity limited to paranuclear inclusions was also found with the Abcam™ anti-SP antibody in the endothelial cells of the olfactory bulb (c, arrowheads) and (d) in the epithelial cells of the choroid plexus (d, arrowheads) (c, d: *scale bars* = 8 µm). Anti-giantin (e) and anti-furin (f) immunoreactivity showed a paranuclear distribution in cerebral endothelial cells (e, f: *scale bar* = 20 µm). Insets : higher magnification of cells indicated by arrow heads. ACE2 immunoreactivity was present in brain endothelial cells (g: *scale bar* = 8 µm). SP was detected in blood vessels labeled with a CD147 receptor antibody (h: *scale bar* = 8 µm).

the lesions of the white matter can be described as CCM.

For the detection of SARS-CoV-2, two different antibodies were used, yielding similar results in the biopsied and autopsied cases. Within the foci, the hemorrhage and cellular debris interfered with a thorough analysis of endothelial cells. However at a short distance from the hemorrhagic foci, both antibodies labelled numerous inclusions in endothelial cells of apparently spared vessels (Fig. 3. a, b). Most positive vessels where observed in the frontal, parietal and temporal white matter, although some labeling was observed in the brain stem and striatum in autopsied cases. With the monoclonal anti-N antibody, immunoreactivity was predominant in endothelial cells, with a diffuse endothelial labelling and para-nuclear enhancement (Fig. 3. a). With the monoclonal antibody directed against SP (Fig. 3. b), the labelling was paranuclear in a topography suggestive of the Golgi apparatus.

In the cortical gray matter, a few SP positive dots were also seen in the endothelial cells, however, no sign of microangiopathy was detected. Thus, CCM appeared to be confined to the white matter. In the olfactory bulb, SP immunoreactivity was detected in the endothelial cells only (Fig. 3. c), as in the other regions of the nervous system. In the choroid plexus, around 20% of the villi's epithelial cells contained SP (Fig. 3. d). The intracellular localization was similar to what was previously seen. No SP was observed in the COVID-19 cases that did not develop brain vascular lesions.

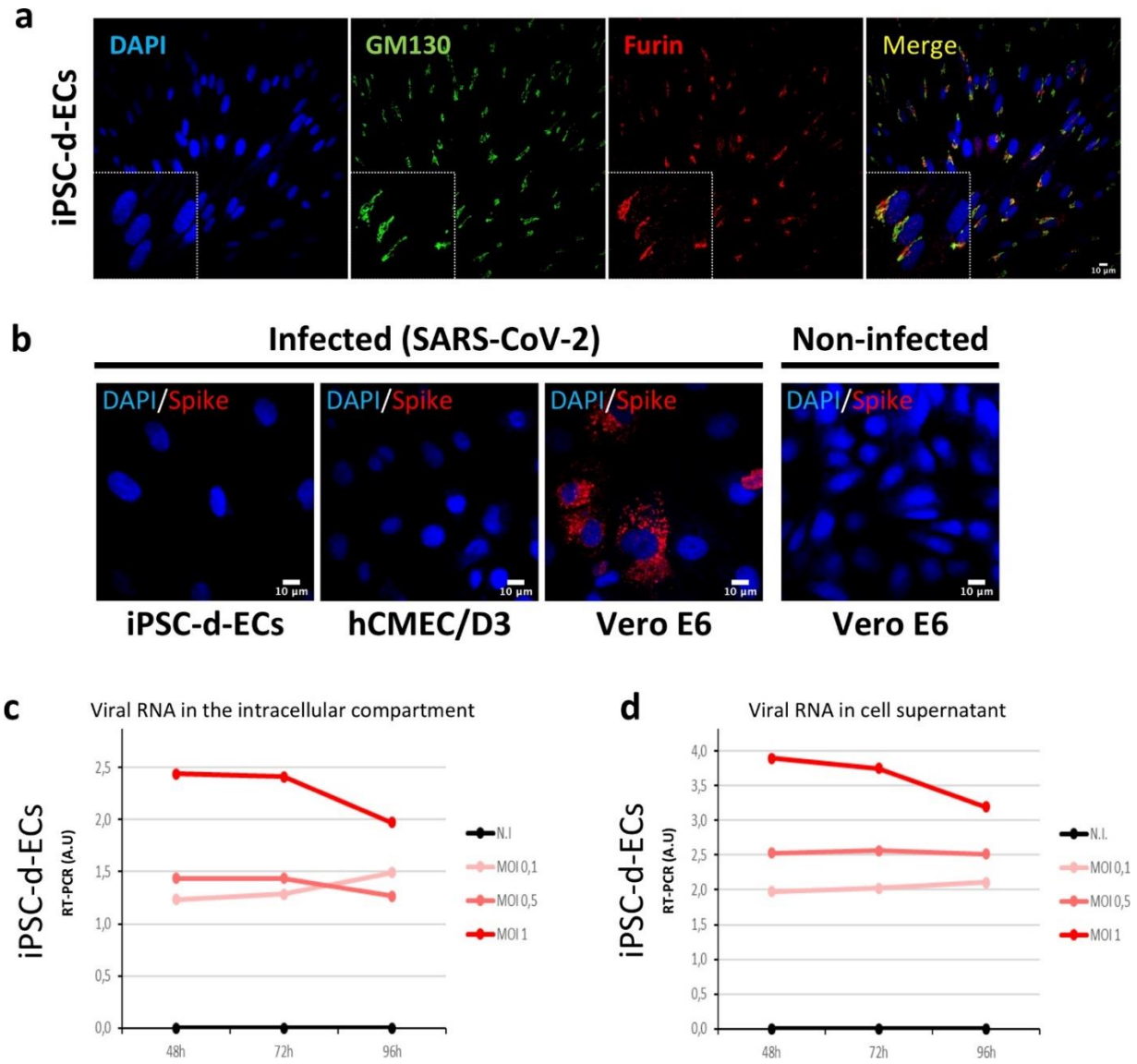

Fig. 4. Human endothelial and Vero E6 cells. (a) Furin immunoreactivity colocalizes with GM130 immunoreactivity in human iPSC-derived endothelial cells (iPSC-d- EC). (b) Vero E6 and Human endothelial cells (iPSC-d-ECs and hCMEC/D3) were infected with SARS-CoV-2 (MOI 0.1, 0.5, 1) for 48, 72 and 96 hours. SP was detected in Vero E6 but not in infected human endothelial cells. The not infected condition is a negative control for the infection (*scale bar* in a and b = 10µm). (c,d) The RT-PCRs were determined over time (48, 72 and 96 hours post-infection) in (c) cell extract or (d) cell supernatant of iPSC derived endothelial cells infected or not with SARS-CoV-2. No evidence of viral RNA amplification was observed.

Absence of viral genome or viral particles in brain parenchyma

Different molecular and histological techniques were used to detect viral genome or viral particles of SARS-CoV-2, all of them with negative results.

RT-PCR was negative in the three brain biopsy samples (cases # 1 to 3). In case # 4, RT-PCR was positive in the lungs, mediastinal and cervical lymph nodes, and spleen, but negative elsewhere, including the different brain samples analyzed (Table 3).

No viral sequence was found by agnostic Next Generation Sequencing (NGS) in the three biopsy samples (cases # 1 to 3). Regarding autopsy case # 4, SARS-CoV-2 sequence was not detected in any of the brain samples tested (frontal, temporal and parietal lobes). Instead, one read of HSV-1 was identified in the frontal lobe. Both SARS-CoV-2 and HSV-1 viral sequences were found in the lung, spleen, lymph node and tongue. *In situ* hybridization (ISH) for SARS-CoV-2 was negative in the brain in case # 4, but positive in the lung where large metaplastic pneumocytes were positive (supplementary material).

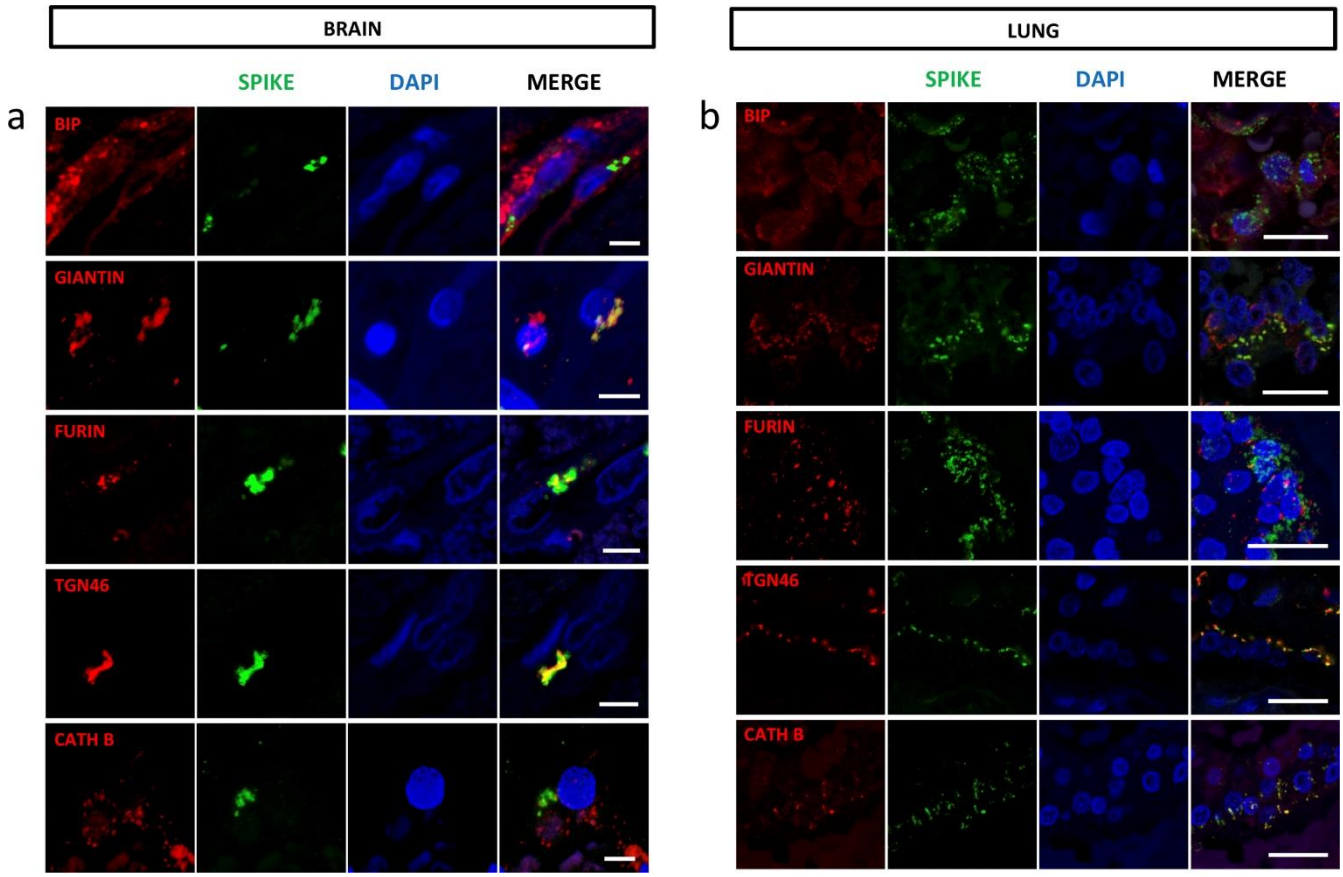

Fig 5. SP localizes to the Golgi apparatus and differs in its distribution between brain and lung. (a) Spike protein colocalizes with giantin, furin and TGN46 in the endothelial cells of brain vessels. First row: BIP protein is seen dispersed throughout the cytoplasm of the endothelial cell and does not colocalize with SP. *Second row:* Giantin immunoreactivity is paranuclear similarly to SP and is found partially colocalizing with SP. *Third row:* Furin is seen in a paranuclear location in endothelial cells and colocalizes with SP. *Fourth row:* TGN46, which localizes next to the nucleus in the endothelial cell, colocalizes with SP. *Fifth row:* Cathepsin B is seen dispersed throughout the cytoplasm of the endothelial cells with no colocalization with SP. (First, third and fourth row: case # 4; Second and fifth row: case # 6; *Scale bars in all rows* = 5µm). **(b) Spike protein colocalizes with TGN46 and Cathepsin B in type II pneumocytes.** *First row:* BIP protein is dispersed throughout the cytoplasm of type II pneumocytes and does not colocalize with SP. *Second row:* Giantin is distributed diffusely in type II pneumocytes and does not colocalize with SP. *Third row:* Furin is seen as fine granular positivity and is dispersed in the cytoplasm of type II pneumocytes. It does not colocalize with SP. *Fourth row:* TGN46 is seen as fine granular diffuse positivity and partially colocalizes with SP. *Fifth row:* Cathepsin B is dispersed throughout the cytoplasm of the endothelial cells and colocalizes partially with SP. (All rows: case # 4) (*Scale bars in all rows* = 20µm).

Lack of detectable viral genome in brain tissue was confirmed with high-amplification and target-specific ISH (RNAscope technology, data not shown). Electron microscopy examination of white matter tissue from case # 4 did not reveal the presence of viral particles. Instead, many clathrin coated particles were identified (data not shown).

SP immunocytochemistry was positive in infected Vero E6 cells (Fig.4. b) but negative in both iPSC-d-ECs and hCMEC/D3 infected cell lines (Fig. 4. b). In addition, SARS-CoV-2 RT-PCRs on samples from the cell culture supernatant and from the intracellular compartment of endothelial cells derived from control iPSC-d-ECs, showed no amplification of the viral RNA either in the cells (Fig. 4. c) or in the supernatant (Fig. 4. d) at the three MOI done. Furthermore, after incubation of HUVEC cells with recombinant SP S1 full length peptide and control RBD peptide, no staining was detected using anti-S1 and anti-RBD antibodies (data not shown), although control VERO E6 cells, infected with SARS-CoV-2 virus, showed immunoreactivity for both anti-S1 and anti-

RBD antibodies. These results suggest that endothelial cells are refractory to SARS-CoV-2 *in vitro* infection.

SP is localized in the Golgi apparatus and is associated with furin

As mentioned above, SP immunoreactivity was paranuclear suggesting a localization of the viral particles in the Golgi apparatus. This was confirmed by giantin and TGN46 immunoreactivity (Fig 3. e & 5. a). Giantin is a protein of the cis-media cisternae and TGN46 is found in the trans-Golgi network. Both proteins were partly colocalized with SP in brain endothelial cells (Fig. 5 a). By contrast, BIP, a protein of the endoplasmic reticulum and cathepsin B, a protein of the lysosomal pathway, did not show colocalization with SP in the brain endothelial cells (Fig. 5 a).

The IHC labelling of furin, which is also a Golgi protein that can migrate into the lysosomal system [29], was detected in the same paranuclear localization as SP in patients (Fig. 3. f) and colocalization of the two proteins was confirmed by confocal microscopy (Fig. 5 a). We then looked for furin immunoreactivity in cases with vascular lesions due to ECMO, amyloid angiopathy or intravascular lymphoma and could not detect furin expression. This ruled out furin expression as a non specific reaction of the endothelium. After infection of iPSC-d-ECs and hCMEC/D3 cell lines we observed that furin was mainly localized in the Golgi apparatus and in cytosolic vesicles (Fig. 4. a). This localization was the same as previously reported [29].

We also investigated the association of ACE2 and CD147/basigin in the vascular lesions of SARS-CoV-2 cases with CCM. ACE2 and CD147/basigin have both been considered receptors of SARS-CoV-2. ACE2 immunoreactivity was seen in most endothelial cells (Fig. 3. g) whereas CD147/basigin was expressed at the luminal surface of endothelial cells in some vessels. Double labeling showed that SP immunoreactivity was present in CD147/basigin positive vessels and in furin positive endothelial cells (Fig 3. h).

The distribution of SP was different between brain and lung. While in the brain SP was compact and had a paranuclear localization limited to the endothelial cells, it was spread as small particles in the cytoplasm of type II pneumocytes of the lung (Fig. 5 a, b). In the brain, SP colocalized with the Golgi proteins: giantin, furin, and TGN46 (Fig. 5. a), while in the lung, colocalization was seen with TGN46 and cathepsin B (Fig 5. b).

Discussion

In six COVID-19 cases with neurological symptoms, multiple microvascular lesions were found in the white matter. They were made of foci of vacuolized tissue with red blood cells, macrophages, axonal swellings, a few T lymphocytes and perivascular fibrinogen deposits. The vessels were not occluded and the alteration of perivascular tissue was different from acute necrosis such as seen in recent lacunae. Perivascular cuffing commonly seen in encephalitides was absent. The small number of lymphocytes was in contrast with the abundance of macrophage infiltration. The high number of macrophages and the absence of polymorphonuclear leukocytes suggest that the lesions occurred at least several days earlier. The absence of myelino-axonal dissociation and of myelin laden macrophages suggested that demyelination was not involved. The nuclear abnormalities in the glial cells observed in the biopsy cases could not be related to a cytopathogenic effect since no viral presence in these cells could be detected with the techniques used. On the other hand, these astrocytes evoke Creutzfeldt-Peters cells, initially described in multiple sclerosis but present, in a non-specific way, in a wide spectrum of cerebral diseases including anoxic encephalopathy [51]. The pattern of AQP4 IHC was different from that described in demyelinating diseases such as multiple sclerosis, *neuromyelitis optica* (NMO) or ADEM [33]. In our cases, AQP4 was strongly expressed by astrocytes at the periphery of the foci. Vacuolization of the perivascular tissue and fibrinogen extravasation were evidence of a blood-brain barrier leakage. In addition to the observations made by Lee et al. [24, 25] (macrophages, few lymphocytes, blood-brain barrier leakage), we stress the presence of axonal injury and astrocytic alterations in the foci.

Arterial damage could be explained by critical care in itself [23]. However these lesions are particularly frequent in COVID-19 patients and may occur in the absence of severe cardiovascular failure or extracorporeal membrane oxygenation (ECMO) [6]. In addition, the presence of SP in the endothelial cell in our patients argues for the specificity of the lesions.

Despite the use of different techniques (RT-PCR, nested-PCR, agnostic and targeted NGS, in situ hybridization, electron microscopy) SARS-CoV-2 viral sequences or particles were not detected in the brain parenchyma, in agreement with previous observations [12, 24, 53]. We could, however, show the presence of viral proteins in the endothelial cells, as Meinhardt et al. who used the same antibody (Abcam, ab272420; 1:100) as us [32]. We could confirm this result with another antibody against the nucleocapsid (Cliniscience). We found an association between the presence of significant SP immunoreactivity in the endothelial cells and the tissue damage. The detection of SP was not limited to the most injured vessels (whose wall was too altered to analyze the endothelial cells) but to the vessels around the regions in which the lesions were observed. These anomalies could be interpreted as a preparation of the vessel for a more severe damage. Our study was limited by the small number of autopsies obtained, that restrained the access to more representative cases of a relatively rare event. When only biopsy was available, the material was not sufficient to reproduce all the techniques. Nevertheless our results suggest that the role of SARS-CoV-2 SP in microangiopathy, described in animal models [38], could apply to humans.

The discrepancy between the presence of SP and nucleocapsid immunoreactivity and the absence of viral genomes suggests that RNA levels were too low at this stage to be detected, while SP and nucleocapsid protein immunoreactivity have persisted after the RNA degradation, several weeks after acute infection.

The detection of these viral proteins in the endothelium and epithelial cells of the choroid plexus suggests that the virus could enter the CNS via the vessels rather than through nerve processes. SP could be transported in the bloodstream, cross the blood brain barrier [46] and enter endothelial cells by endocytosis [38]. Nevertheless, the hypothesis of an isolated protein transport seems implausible given the presence not only of SP but also of nucleocapsid protein in the endothelial cells. In addition, our attempts to incubate recombinant SP S1 full length peptide with HUVEC cells did not lead to internalization of the protein. In cell culture, neither the virus nor the SP could not penetrate the endothelial cells, in accordance with recent data from the literature [1, 30, 35], suggesting that endothelial cells are refractory to SARS-CoV-2 *in vitro* infection. Both CD147/basigin and ACE2 were expressed in the iPSC-d-EC and hCMEC/D3 lines underlining that resistance to infection was not due to the absence of these receptors. We are aware that our models do not fully account for the brain endothelial cell behavior towards SARS-CoV-2 infection, since they were not specific for this type of cells and did not reproduce the complex structure and function of the blood-brain barrier.

However, we propose that the vascular abnormalities we observed are related to peculiarities of pathways followed by the virus once it has entered a cerebral endothelial cell, precluding its subsequent replication. The paranuclear topography of SP1 and its association with giantin and TGN46 are evidence that SP molecules were located in the Golgi apparatus. The Golgi and trans-Golgi immunoreactivity was in strong contrast with that observed in the lung where there was colocalization between SP not only with TGN46 but also with cathepsin B, a lysosomal marker, suggesting that SP follows a complete cycle of replication in the lung. Thus, it appears that the metabolism of SP is different in brain endothelial cells and in pneumocytes. In the latter, the virions egress from the cell by a lysosomal pathway [14]. In the former, SP accumulates in the Golgi and trans-Golgi network. The cause of the differential use of these pathways and their impact on pathology remains to be further explored.

Since the start of the present study, several papers have proposed mechanisms leading to SARS-CoV-2 specific vascular lesions. SARS-CoV-2 protein (M^{pro}) could interact with the host protein nuclear factor NF-κB essential modulator (NEMO), which is part of the signaling cascade that regulates the transcription of several genes, some of which are involved in inflammation [57]. Other authors have identified an SP (Spike)-triggered transcriptional re-

sponse associated with extracellular matrix reorganization and TGF-β signaling [3]. We have found colocalization of SP immunoreactivity with furin protease in the trans-Golgi network. Our observations suggest that SP, in association with furin and possibly other molecules, may play a role in the development of vascular pathologies. Among the genomic features that differentiate SARS-CoV-2 from the other members of the CoV family, the insertion of four amino acid residues (PRRA) at the junction of the S1 and S2 subunits of SP has generated a cleavage site for furin and other proteases [9]. Furin inactivation has been shown to decrease SARS-CoV-2 infectivity, virus production and cytopathic effect [5, 19]. Besides its role in SARS-CoV-2 infectivity, furin is highly expressed in vascular endothelial cells and modulates endothelial permeability [29]. Furin has been considered as a possible therapeutic target [19]. Inhibition of furin may indeed have a protective effect against hypoxia and blood brain barrier disruption [2, 31].

These observations not only shed light on the neurological lesions observed in some COVID-19 patients in the acute phase but may provide insight into the mechanism of later onset dysfunction. A network-based approach linked cerebral microvascular lesions to late cognitive impairment after the COVID-19 episode, suggesting that microangiopathy could have long-term consequences [58].

In conclusion, we have defined additional histological characteristics of CCM associated with leakage of the blood brain barrier: foci of vacuolized white matter, axonal swellings, AQP4 redistribution in astrocytes. We detected the presence of SP in the trans-Golgi network associated with furin protease. The accumulation of SP in the Golgi of endothelial cells was in contrast with the aspect of infected pneumocytes in which SP and nucleocapsid protein immunoreactivity was spread in the whole cell body. The difference in the metabolism of the virus in the two cell types explain the differences in pathogenic effect. In the brain, the tight association between SP and furin suggests that their interaction is involved in the pathogenesis of COVID associated microangiopathy. The late effects of the microangiopathy are not known. As furin plays a role in the modulation of vascular permeability, our findings may provide further arguments in the control of late effects of microangiopathy.

Acknowlegments

We thank the patients and their family. The authors thank the Cohort COVID-19 Neurosciences (CoCo Neurosciences) study supported by APHP and funded by the generous support of the Federation Internationale de l'Automobile (FIA), the FIA Foundation and donors of Paris Brain Institute – ICM. The authors thank the CoCo-Neurosciences study group for their participation to data collection and Pierre Rufat for his valuable contribution. The research leading to these results has received funding from Sorbonne University (PathoCoV project) and from the program "Investissements d'avenir" ANR-10-IAIHU-06. We thank the staff of the Raymond Escourolle neuropathology laboratory for their commitment into the project. Parts of the histological work-analysis were performed on the HISTOMICS and ICM.QUANT platforms of the Paris brain institute (ICM), we thank all technical staff involved. This work benefited from equipment and services from the CELIS cell culture core facility (Paris Brain Institute), a platform receiving support from ANR-10-IAIHU-06 and ANR-11-INBS-0011-NeurATRIS. We thank for targeted NGS sequencing the Biomics Platform, C2RT, Institut Pasteur, Paris, France, supported by France Génomique (ANR-10-INBS-09-09), IBISA and the Illumina COVID-19 Projects' offer.

References

1 Ahmetaj-Shala B, Peacock TP, Baillon L, Swann OC, Gashaw H, Barclay WS, Mitchell JA (2020) Resistance of endothelial cells to SARS-CoV-2 infection in vitro. bioRxiv: 2020.2011.2008.372581. https://doi.org/10.1101/2020.11.08.372581

2 Baumann J, Huang SF, Gassmann M, Tsao CC, Ogunshola OO (2019) Furin inhibition prevents hypoxic and TGFbeta-mediated blood-brain barrier disruption. Exp Cell Res 383: 111503. https://doi.org/10.1016/j.yexcr.2019.111503

3 Biering SB, Gomes de Sousa FT, Tjang LV, Pahmeier F, Zhu C, Ruan R, Blanc SF, Patel TS, Worthington CM, Glasner DR et al (2022) SARS-CoV-2 Spike triggers barrier dysfunction and vascular leak via integrins and TGF-β signaling. Nat Commun 13: 7630. https://doi.org/10.1038/s41467-022-34910-5

4 Cao A, Rohaut B, Le Guennec L, Saheb S, Marois C, Altmayer V, Carpentier VT, Nemlaghi S, Soulie M, Morlon Q et al (2020) Severe COVID-19-related encephalitis can respond to immunotherapy. Brain 143: e102. https://doi.org/10.1093/brain/awaa337

5 Cheng YW, Chao TL, Li CL, Chiu MF, Kao HC, Wang SH, Pang YH, Lin CH, Tsai YM, Lee WH et al (2020) Furin Inhibitors Block SARS-CoV-2 Spike Protein Cleavage to Suppress Virus Production and Cytopathic Effects. Cell Rep 33: 108254. https://doi.org/10.1016/j.celrep.2020.108254

6 Chougar L, Shor N, Weiss N, Galanaud D, Leclercq D, Mathon B, Belkacem S, Stroer S, Burrel S, Boutolleau D et al (2020) Retrospective Observational Study of Brain MRI Findings in Patients with Acute SARS-CoV-2 Infection and Neurologic Manifestations. Radiology 297: E313-E323. https://doi.org/10.1148/radiol.2020202422

7 Coolen T, Lolli V, Sadeghi N, Rovaï A, Trotta N, Taccone FS, Creteur J, Henrard S, Goffard JC, De Witte O et al (2020) Early postmortem brain MRI findings in COVID-19 non-survivors. Neurology 95 (14): e2016-e2027. https://doi.org/10.1212/WNL.0000000000010116

8 Corrêa DG, de Souza Lima FC, da Cruz Bezerra D, Coutinho AC, Hygino da Cruz LC (2020) COVID-19 associated with encephalomyeloradiculitis and positive anti-aquaporin-4 antibodies: Cause or coincidence? Mult Scler: 1352458520949988. https://doi.org/10.1177/1352458520949988

9 Coutard B, Valle C, de Lamballerie X, Canard B, Seidah NG, Decroly E (2020) The spike glycoprotein of the new coronavirus 2019-nCoV contains a furin-like cleavage site absent in CoV of the same clade. Antiviral Res 176: 104742. https://doi.org/10.1016/j.antiviral.2020.104742

10 Egervari K, Thomas C, Lobrinus JA, Kuhlmann T, Bruck W, Love S, Crary JF, Stadelmann C, Paulus W, Merkler D (2021) Neuropathology associated with SARS-CoV-2 infection. Lancet 397: 276-277. https://doi.org/10.1016/S0140-6736(21)00095-7

11 Ellul MA, Benjamin L, Singh B, Lant S, Michael BD, Easton A, Kneen R, Defres S, Sejvar J, Solomon T (2020) Neurological associations of COVID-19. Lancet Neurol 19: 767-783. https://doi.org/10.1016/S1474-4422(20)30221-0

12 Eschbacher KL, Larsen RA, Moyer AM, Majumdar R, Reichard RR (2022) Neuropathological findings in COVID-19: an autopsy cohort. Journal of Neuropathology & Experimental Neurology 82: 21-28. https://doi.org/10.1093/jnen/nlac101

13 Fotuhi M, Mian A, Meysami S, Raji CA (2020) Neurobiology of COVID-19. J Alzheimers Dis 76: 3-19. https://doi.org/10.3233/jad-200581

14 Ghosh S, Dellibovi-Ragheb TA, Kerviel A, Pak E, Qiu Q, Fisher M, Takvorian PM, Bleck C, Hsu VW, Fehr AR et al (2020) β-Coronaviruses Use Lysosomes for Egress Instead of the Biosynthetic Secretory Pathway. Cell 183: 1520-1535.e1514. https://doi.org/10.1016/j.cell.2020.10.039

15 Glatzel M, Hagel C, Matschke J, Sperhake J, Deigendesch N, Tzankov A, Frank S (2021) Neuropathology associated with SARS-CoV-2 infection. Lancet 397: 276. https://doi.org/10.1016/s0140-6736(21)00098-2

16 Hernández-Fernández F, Valencia HS, Barbella-Aponte RA, Collado-Jiménez R, Ayo-Martín Ó, Barrena C, Molina-Nuevo JD, García-García J, Lozano-Setién E, Alcahut-Rodriguez C et al (2020) Cerebrovascular disease in patients with COVID-19: neuroimaging, histological and clinical description. Brain 143: 3089-3103. https://doi.org/10.1093/brain/awaa239

17 Hoffmann M, Kleine-Weber H, Schroeder S, Krüger N, Herrler T, Erichsen S, Schiergens TS, Herrler G, Wu NH, Nitsche A et al (2020) SARS-CoV-2 Cell Entry Depends on ACE2 and TMPRSS2 and Is Blocked by a Clinically Proven Protease Inhibitor. Cell 181: 271-280. https://doi.org/10.1016/j.cell.2020.02.052

18 Jaunmuktane Z, Mahadeva U, Green A, Sekhawat V, Barrett NA, Childs L, Shankar-Hari M, Thom M, Jäger HR, Brandner S (2020) Microvascular injury and hypoxic damage: emerging neuropathological signatures in COVID-19. Acta Neuropathol 140: 397-400. https://doi.org/10.1007/s00401-020-02190-2

19 Johnson BA, Xie X, Bailey AL, Kalveram B, Lokugamage KG, Muruato A, Zou J, Zhang X, Juelich T, Smith JK et al (2021) Loss of furin cleavage site attenuates SARS-CoV-2 pathogenesis. Nature 591: 293-299. https://doi.org/10.1038/s41586-021-03237-4

20 Johnson BA, Xie X, Kalveram B, Lokugamage KG, Muruato A, Zou J, Zhang X, Juelich T, Smith JK, Zhang L et al (2020) Furin cleavage site is key to SARS-CoV-2 pathogenesis. bioRxiv: 08.26.268854. https://doi.org/10.1101/2020.08.26.268854

21 Kirschenbaum D, Imbach LL, Rushing EJ, Frauenknecht KBM, Gascho D, Ineichen BV, Keller E, Kohler S, Lichtblau M, Reimann RR et al (2020) Intracerebral endotheliitis and microbleeds are neuropathological features of COVID-19. Neuropathol Appl Neurobiol 47: 454-459. https://doi.org/10.1111/nan.12677

22 Kremer S, Lersy F, de Sèze J, Ferré JC, Maamar A, Carsin-Nicol B, Collange O, Bonneville F, Adam G, Martin-Blondel G et al (2020) Brain MRI findings in severe COVID-19: A retrospective observational study. Radiology 297: E242-E251. https://doi.org/10.1148/radiol.2020202222

23 Le Guennec L, Cholet C, Huang F, Schmidt M, Bréchot N, Hékimian G, Besset S, Lebreton G, Nieszkowska A, Leprince P et al (2018) Ischemic and hemorrhagic brain injury during venoarterial-extracorporeal membrane oxygenation. Ann Intensive Care 8: 129. https://doi.org/10.1186/s13613-018-0475-6

24 Lee MH, Perl DP, Nair G, Li W, Maric D, Murray H, Dodd SJ, Koretsky AP, Watts JA, Cheung V et al (2020) Microvascular injury in the brains of patients with Covid-19. N Engl J Med 384: 481-483. https://doi.org/10.1056/NEJMc2033369

25 Lee MH, Perl DP, Steiner J, Pasternack N, Li W, Maric D, Safavi F, Horkayne-Szakaly I, Jones R, Stram MN et al (2022) Neurovascular injury with complement activation and inflammation in COVID-19. Brain 145: 2555-2568. https://doi.org/10.1093/brain/awac151

26 Majidi S, Fifi JT, Ladner TR, Lara-Reyna J, Yaeger KA, Yim B, Dangayach N, Oxley TJ, Shigematsu T, Kummer BR et al (2020) Emergent large vessel occlusion stroke during New York City's COVID-19 outbreak: clinical characteristics and paraclinical findings. Stroke 51: 2656-2663. https://doi.org/10.1161/strokeaha.120.030397

27 Mao L, Jin H, Wang M, Hu Y, Chen S, He Q, Chang J, Hong C, Zhou Y, Wang D et al (2020) Neurologic Manifestations of Hospitalized Patients With Coronavirus Disease 2019 in Wuhan, China. JAMA Neurol 77: 683-690. https://doi.org/10.1001/jamaneurol.2020.1127

28 Matschke J, Lütgehetmann M, Hagel C, Sperhake JP, Schröder AS, Edler C, Mushumba H, Fitzek A, Allweiss L, Dandri M et al (2020) Neuropathology of patients with COVID-19 in Germany: a post-mortem case series. Lancet Neurol 19: 919-929. https://doi.org/10.1016/s1474-4422(20)30308-2

29 Mayer G, Boileau G, Bendayan M (2004) Sorting of furin in polarized epithelial and endothelial cells: expression beyond the Golgi apparatus. J Histochem Cytochem 52: 567-579. https://doi.org/10.1177/002215540405200502

30 McCracken IR, Saginc G, He L, Huseynov A, Daniels A, Fletcher S, Peghaire C, Kalna V, Andaloussi-Mäe M, Muhl L et al (2021) Lack of evidence of angiotensin-converting enzyme 2 expression and replicative infection by SARS-CoV-2 in human endothelial cells. Circulation 143: 865-868. https://doi.org/10.1161/circulationaha.120.052824

31 McMillin MA, Frampton GA, Seiwell AP, Patel NS, Jacobs AN, DeMorrow S (2015) TGFβ1 exacerbates blood-brain barrier permeability in a mouse model of hepatic encephalopathy via upregulation of MMP9 and downregulation of claudin-5. Lab Invest 95: 903-913. https://doi.org/10.1038/labinvest.2015.70

32 Meinhardt J, Radke J, Dittmayer C, Franz J, Thomas C, Mothes R, Laue M, Schneider J, Brünink S, Greuel S et al (2020) Olfactory transmucosal SARS-CoV-2 invasion as a port of central nervous system entry in individuals with COVID-19. Nat Neurosci 24: 168-175. https://doi.org/10.1038/s41593-020-00758-5

33 Misu T, Fujihara K, Kakita A, Konno H, Nakamura M, Watanabe S, Takahashi T, Nakashima I, Takahashi H, Itoyama Y (2007) Loss of aquaporin 4 in lesions of neuromyelitis optica: distinction from multiple sclerosis. Brain 130: 1224-1234. https://doi.org/10.1093/brain/awm047

34 Moriguchi T, Harii N, Goto J, Harada D, Sugawara H, Takamino J, Ueno M, Sakata H, Kondo K, Myose N et al (2020) A first case of meningitis/encephalitis associated with SARS-Coronavirus-2. Int J Infect Dis 94: 55-58. https://doi.org/10.1016/j.ijid.2020.03.062

35 Nascimento Conde J, Schutt WR, Gorbunova EE, Mackow ER (2020) Recombinant ACE2 Expression Is Required for SARS-CoV-2 To Infect Primary Human Endothelial Cells and Induce Inflammatory and Procoagulative Responses. mBio 11: e03185-03120. https://doi.org/10.1128/mBio.03185-20

36 Natoli S, Oliveira V, Calabresi P, Maia LF, Pisani A (2020) Does SARS-Cov-2 invade the brain? Translational lessons from animal models. Eur J Neurol 27: 1764-1773. https://doi.org/10.1111/ene.14277

37 Novi G, Rossi T, Pedemonte E, Saitta L, Rolla C, Roccatagliata L, Inglese M, Farinini D (2020) Acute disseminated encephalomyelitis after SARS-CoV-2 infection. Neurol Neuroimmunol Neuroinflamm 7: e797. https://doi.org/10.1212/nxi.0000000000000797

38 Nuovo GJ, Magro C, Shaffer T, Awad H, Suster D, Mikhail S, He B, Michaille JJ, Liechty B, Tili E (2020) Endothelial cell damage is the central part of COVID-19 and a mouse model induced by injection of the S1 subunit of the spike protein. Ann Diagn Pathol 51: 151682. https://doi.org/10.1016/j.anndiagpath.2020.151682

39 Ou X, Liu Y, Lei X, Li P, Mi D, Ren L, Guo L, Guo R, Chen T, Hu J et al (2020) Characterization of spike glycoprotein of SARS-CoV-2 on virus entry and its immune cross-reactivity with SARS-CoV. Nat Commun 11: 1620. https://doi.org/10.1038/s41467-020-15562-9

40 Oxley TJ, Mocco J, Majidi S, Kellner CP, Shoirah H, Singh IP, De Leacy RA, Shigematsu T, Ladner TR, Yaeger KA et al (2020) Large-vessel stroke as a presenting feature of Covid-19 in the young. N Engl J Med 382: e60. https://doi.org/10.1056/NEJMc2009787

41 Patsch C, Challet-Meylan L, Thoma EC, Urich E, Heckel T, O'Sullivan JF, Grainger SJ, Kapp FG, Sun L, Christensen K et al (2015) Generation of vascular endothelial and smooth muscle cells from human pluripotent stem cells. Nat Cell Biol 17: 994-1003. https://doi.org/10.1038/ncb3205

42 Pérot P, Bielle F, Bigot T, Foulongne V, Bolloré K, Chrétien D, Gil P, Gutiérrez S, L'Ambert G, Mokhtari K et al (2020) Identification of Umbre orthobunyavirus as a novel zoonotic virus responsible for lethal encephalitis in 2 French patients with hypogammaglobulinemia. Clin Infect Dis 72: 1701-1708. https://doi.org/10.1093/cid/ciaa308

43 Poyiadji N, Shahin G, Noujaim D, Stone M, Patel S, Griffith B (2020) COVID-19-associated acute hemorrhagic necrotizing encephalopathy: CT and MRI features. Radiology 296: E119-E120. https://doi.org/10.1148/radiol.2020201187

44 Redwan EM, Elrashdy F, Aljabali AAA, Baetas-da-Cruz W, Barh D, Brufsky AM, Hassan SS, Lundstrom K, Serrano-Aroca Á, Takayama K et al (2022) Would New SARS-CoV-2 Variants Change the War against COVID-19? Epidemiologia 3: 229-237. https://doi.org/10.3390/epidemiologia3020018

45 Reichard RR, Kashani KB, Boire NA, Constantopoulos E, Guo Y, Lucchinetti CF (2020) Neuropathology of COVID-19: a spectrum of vascular and acute disseminated encephalomyelitis (ADEM)-like pathology. Acta Neuropathol 140: 1-6. https://doi.org/10.1007/s00401-020-02166-2

46 Rhea EM, Logsdon AF, Hansen KM, Williams LM, Reed MJ, Baumann KK, Holden SJ, Raber J, Banks WA, Erickson MA (2021) The S1 protein of SARS-CoV-2 crosses the blood-brain barrier in mice. Nat Neurosci 24: 368-378. https://doi.org/10.1038/s41593-020-00771-8

47 Serrano GE, Walker JE, Arce R, Glass MJ, Vargas D, Sue LI, Intorcia AJ, Nelson CM, Oliver J, Papa J et al (2021) Mapping of SARS-CoV-2 brain invasion and histopathology in COVID-19 disease. medRxiv: 02.15.21251511. https://doi.org/10.1101/2021.02.15.21251511

48 Shang J, Wan Y, Luo C, Ye G, Geng Q, Auerbach A, Li F (2020) Cell entry mechanisms of SARS-CoV-2. Proc Natl Acad Sci U S A 117: 11727-11734. https://doi.org/10.1073/pnas.2003138117

49 Solomon IH, Normandin E, Bhattacharyya S, Mukerji SS, Keller K, Ali AS, Adams G, Hornick JL, Padera RF, Jr., Sabeti P (2020) Neuropathological Features of Covid-19. N Engl J Med 383: 989-992. https://doi.org/10.1056/NEJMc2019373

50 Song E, Zhang C, Israelow B, Lu-Culligan A, Prado AV, Skriabine S, Lu P, Weizman OE, Liu F, Dai Y et al (2021) Neuroinvasion of SARS-CoV-2 in human and mouse brain. J Exp Med 218: e20203135. https://doi.org/10.1084/jem.20202135

51 Sosunov A, Wu X, McGovern R, Mikell C, McKhann GM, 2nd, Goldman JE (2020) Abnormal mitosis in reactive astrocytes. Acta Neuropathol Commun 8: 47. https://doi.org/10.1186/s40478-020-00919-4

52 Stein SR, Ramelli SC, Grazioli A, Chung J-Y, Singh M, Yinda CK, Winkler CW, Sun J, Dickey JM, Ylaya K et al (2022) SARS-CoV-2 infection and persistence in the human body and brain at autopsy. Nature 612: 758-763. https://doi.org/10.1038/s41586-022-05542-y

53 Thakur KT, Miller EH, Glendinning MD, Al-Dalahmah O, Banu MA, Boehme AK, Boubour AL, Bruce SS, Chong AM, Claassen J et al (2021) COVID-19 neuropathology at Columbia University Irving Medical Center/New York Presbyterian Hospital. Brain 144: 2696-2708. https://doi.org/10.1093/brain/awab148

54 von Weyhern CH, Kaufmann I, Neff F, Kremer M (2020) Early evidence of pronounced brain involvement in fatal COVID-19 outcomes. Lancet 395: e109. https://doi.org/10.1016/s0140-6736(20)31282-4

55 Weksler B, Romero IA, Couraud P-O (2013) The hCMEC/D3 cell line as a model of the human blood brain barrier. Fluids and Barriers of the CNS 10: 16. https://doi.org/10.1186/2045-8118-10-16

56 Weksler BB, Subileau EA, Perrière N, Charneau P, Holloway K, Leveque M, Tricoire-Leignel H, Nicotra A, Bourdoulous S, Turowski P et al (2005) Blood-brain barrier-specific properties of a human adult brain endothelial cell line. Faseb j 19: 1872-1874. https://doi.org/10.1096/fj.04-3458fje

57 Wenzel J, Lampe J, Müller-Fielitz H, Schuster R, Zille M, Müller K, Krohn M, Körbelin J, Zhang L, Özorhan Ü et al (2021) The SARS-CoV-2 main protease M(pro) causes microvascular brain pathology by cleaving NEMO in brain endothelial cells. Nat Neurosci 24: 1522-1533. https://doi.org/10.1038/s41593-021-00926-1

58 Zhou Y, Xu J, Hou Y, Leverenz JB, Kallianpur A, Mehra R, Liu Y, Yu H, Pieper AA, Jehi L et al (2021) Network medicine links SARS-CoV-2/COVID-19 infection to brain microvascular injury and neuroinflammation in dementia-like cognitive impairment. Alzheimers Res Ther 13: 110. https://doi.org/10.1186/s13195-021-00850-3